ADVANCES IN SURFACE ENGINEERING

# Molecular Dynamics Investigation of Nanometric Cutting of Single-Crystal Silicon Using a Blunt Tool

SEYED NADER AMELI KALKHORAN [1,2,3] MEHRDAD VAHDATI [1]
and JIWANG YAN [2]

1.—Department of Mechanical Engineering, K.N. Toosi University of Technology, Pardis St., Vanak Sq, Tehran, Iran. 2.—Department of Mechanical Engineering, Keio University, Hiyoshi 3-14-1, Kohoku-ku, Yokohama 223-8522, Japan. 3.—e-mail: Naderameli@mail.kntu.ac.ir

A cutting process is strongly affected by depth of cut ($h_0$) and tool edge radius ($r_e$), the relationship of which is described by relative tool sharpness (RTS = $h_0/r_e$). In nanometric cutting, the depth of cut is far smaller than the tool edge radius, thus the tool is actually a very blunt one with a highly negative effective tool rake angle ($\sim -90°$). However, most previous studies have assumed the tool is extremely sharp with a nanometric edge radius, and to date there is very little literature on the cutting mechanism for a blunt tool (RTS < 1). In this study, the material deformation/removal behavior and forces under a small RTS from 1 to 0 were investigated via molecular dynamics. The results show that the surface integrity and chip formation are strongly affected by RTS. As RTS is reduced to 0.25 or smaller, rubbing and ploughing occur with no material removal. In such a circumstance, the force angle drops sharply with remarkable subsurface damage formation in the workpiece. These findings are distinctly different from the common belief, and provide new information for the optimization of the silicon wafer manufacturing process.

## INTRODUCTION

The last two decades have witnessed an enormous growth in demand for products with nano-scale precision. Among various processes, nanometric cutting is one of the advanced techniques which is widely used in the industries, such as optics, micro-sensors, and nano-electronics.[1] With the aid of this process, an ultra-precision workpiece with nano-metric surface roughness is achievable. Even though machining of brittle materials has always been a challenge, silicon parts with the optical surface are extensively required in electronic and infrared optical devices.[2]

The undeformed chip thickness in nanometric cutting is mostly smaller than the edge radius of a commercially available diamond tool. Thus, the tool is in fact a very blunt one with a highly negative effective tool rake angle ($\sim -90°$). To describe the relationship of undeformed chip thickness and edge radius, relative tool sharpness (RTS) has been presented below:[3]

$$\text{RTS} = \frac{h_0}{r_e} \tag{1}$$

in which $h_0$ is the undeformed chip thickness and $r_e$ the tool edge radius.

RTS affects the cutting mechanism, energy dissipation, residual stress, tool life, and other aspects of the cutting process. RTS is reduced to 0.3 in micromachining and even less than 0.1 in nanomachining.[4] In abrasive machining processes, such as grinding, lapping and polishing of silicon wafers, the abrasive grain size is usually far larger than the machining scale. This is very similar to the situation of cutting with a blunt tool.

A number of previous studies were carried out to experimentally investigate the cutting mechanisms at an extremely small undeformed chip thickness with consideration of the tool edge radius, and found significantly different phenomena from conventional cutting.[5–8] They used various minimum depths of cut in silicon machining. However, almost all the results were only obtained with a specific tool

edge radius, and the effect of RTS was not considered. They also showed that increases in undeformed chip thickness results in a decreasing force angle.

The effect of RTS has been experimentally investigated by a few researchers.[9–12] They introduced the range of 0.13–0.4 for the minimum RTS at which chip formation could occur, although the focus was mostly on investigating brittle–ductile transition, and different RTS values were applied only by variation in the depth of cut (in a constant tool edge radius) using plunge cutting tests.[13] However, previous research did not focus on the different cutting mechanisms during ductile mode at nanometric depth of cut. In addition, it is extremely difficult to observe the material deformation and chip formation behavior by experimental methods because the extremely small machining scale and highly negative rake angle. It is also very tough to measure the cutting forces and examine the subsurface damage generation in the workpiece.

Some researchers have used the finite element method (FEM) to perform machining studies to investigate the effect of tool edge radius on ductile mode machining of silicon.[14] They have investigated phase transformation of silicon due to hydrostatic pressure and the effects of tool edge radius (RTS reduction) on the thrust force (force angle). Nevertheless, the FEM method is not suitable for nanoscale investigations, due to the assumption of continuity and differences in materials properties on nanoscale dimensions.[15] Therefore, the molecular dynamics (MD) method has been introduced as a powerful tool in nanoscale studies, and especially nanometric machining. Komanduri et al.[16] stated that, when the ratio of tangential force to thrust force is less than 1, a shearing mechanism occurs, and when this ratio is within the range of 2, the process behavior is like grinding and the extrusion mechanism will happen. A similar concept was presented by Cai et al.[17] in 2007. The MD method was used by Oluwajobi and Chen[18] to investigate the effect of three different tool edges on the rubbing and ploughing mechanism. The results showed that a trapezoidal tool has the lowest cutting force. It was also revealed that there is no rubbing phenomenon up to a depth of cut of 0.5 Å. Fang et al.[19] used MD simulation to show that, when the depth of cut is 1 nm, an extrusion mechanism occurs. Lai et al.[20] examined the effect of rake angle on the nanometric cutting of copper. They showed that the minimum rake angle for chip formation is − 70°. They also determined that the effective rake angle would depend only on the depth of cut. Goel et al.[21] used 4 different indenter shapes to find the mechanism of deformation in polycrystalline and single-crystal silicon. Their results demonstrated that high-pressure phase transformation is the main mechanism which occurred in all the situations. Balogun et al.[22] used different RTS ratios in a set of side-milling tests to investigate ploughing and shearing mechanisms. They outlined that the best $h/r_e$ ratio is equal to 1 and that in this condition the shearing mechanism is dominant. Ren et al.[23] examined various dimensions and geometries using the molecular dynamics technique. They indicated that the minimum tool feed rate, in which the previous cutting path is not affected, is equal to 5.7 nm for a single-crystal copper workpiece.

Most of the studies on MD simulation of nanometric cutting of silicon have been taken regardless of RTS. In addition, to date, there is very little literature on the cutting mechanism for a blunt tool (RTS < 1), and especially with the simultaneous change of $h_0$ and $r_e$. As a result, surface generation mechanisms (rubbing, ploughing, extrusion and shearing) is poorly understood for a blunt tool.

This work intends to investigate the effect of 6 different RTS ratios lower than 1 on the cutting mechanism using the molecular dynamics simulation method. These RTS values have been produced and studied, not only by changing the tool radius nor depth of cut but also by simultaneously changing both of these parameters. Especially, the surface deformation and chip formation mechanism and subsurface damage formation are investigated under very small RTS, i.e., for a blunt tool. Furthermore, the tangential and thrust force, average forces and force angle are compared in each RTS ratio. With the aid of these results, we can identify the critical values of RTS for cutting mode transition and optimize cutting conditions for the best surface quality. The results will also provide insights for the abrasive machining mechanisms of silicon wafers.

## SIMULATION METHODOLOGY

### Geometric Conditions of Nanometric Machining

Figure 1 shows the scheme of the MD simulation model. The initial temperature of the system is equal to the room temperature (298 K). The workpiece in the simulation model is a single-crystal silicon. It was assumed to be in perfect cubic diamond configuration with the lattice constant of 5.431 Å.[24] Its size is 38.017 (length) × 19.0085
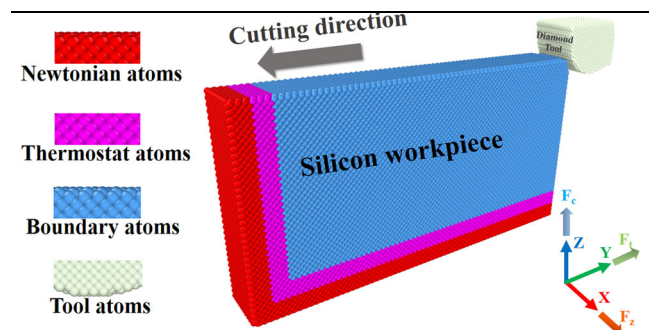


Fig. 1. Schematic description of nanometric cutting model.

(height) × 5.431 (width) nm$^3$ with 198,110 atoms and without any defects. The workpiece is composed of three kinds of atoms: boundary atoms, thermostat atoms, and Newtonian atoms, as shown in Fig. 1. The first region consists of three fixed layers at the bottom and left of the workpiece (red-colored atoms). The purpose of defining these atoms is to prevent the movement of the workpiece during the cutting process. The next three atomic layers placed above these atoms are thermostatic atoms (purple-colored atoms). These atoms imitate the heat dissipation by the chips and coolants during the cutting process.[25] The temperature of this area is kept at a constant temperature of 298 K (equal to the initial temperature of the system) by the velocity-scaling method at every 10 steps. This is a standard method for keeping the temperature of this area constant which has been used by many researchers.[26–28] The remaining workpiece atoms shown in blue are the Newtonian atoms. These atoms are deformable and behave according to the tool movement and problem conditions. This is the main area during the cutting process. The periodic boundary condition is used for the workpiece in the $x$ direction.

Typically, a single point diamond tool is used in the actual process as the cutter. In fact, the resistance of the diamond tool is much higher than that of the silicon workpiece. Hence, a rigid diamond tool with the rake angle and clearance angle of $-10°$ and $15°$, respectively, is used in this investigation.

In order to investigate the effect of RTS ratios lower than 1, the combination of tool edge radii and different depths of cut are employed according to supplementary table SI. According to this table, the various RTS ratios are studied in 6 values of 0, 0.1, 0.25, 0.5, 0.75 and 1. As is shown, these values are deployed by changing both the tool edge radius and depth of cut. This arrangement allows the comparison of the cutting conditions in a specific RTS, but in different conditions (edge radius and depth of cutting). The cutting velocity of 100 m/s is used in this work as an applicable amount to avoid shock wave entrance, and also proceeding with the process up to the desirable span of time. On this basis, the cutting distance for all the simulations was set as 20 nm. In such a cutting length, the process gets stable and the intended phenomena can be examined.

## Interatomic Potential Function

It can be stated that the most critical factor in determining the results of a molecular dynamics simulation is how to define the particles. In physics, analytic potential functions are used to define these interactions. In this study, there are three types of atomic interactions: Si–Si, Si–C, and C–C. A semi-empirical Tersoff potential function is employed in this research to describe the interaction between the silicon atoms. This is one of the most popular potential functions for describing covalently bounded systems like silicon and is based on the concept of bond strength-dependence on the local environment. The interatomic potential is taken to have the form:[29,30]

$$E = \sum_i E_i = \frac{1}{2}\sum_i \sum_{j \neq i} U(r_{ij})$$

$$U(r_{ij}) = f_c(r_{ij})\big[a_{ij}f_R(r_{ij}) + b_{ij}f_A(r_{ij})\big]$$

(2)

where $E$ is the total energy of the system, which is decomposed for convenience into a site energy $E_i$ and a bond energy $U(r_{ij})$.

Even though a large number of researchers have used two-body interactions for workpiece-tool atoms and have considered it is good enough,[31,32] a three-body Tersoff potential function is applied in our models. Moreover, the C–C interaction of the diamond tool is ignored because of the rigid body attribute.

## Simulation Strategy

Despite the definition of the workpiece atoms under real conditions, the system was subjected to two steps of minimization and one equilibrium step. This is due to locating the particles in the perfect structure under the simulation conditions. For this purpose, in the first step, after the definition of the workpiece and the tool, the minimization algorithm was applied. Then, the tool moved to the desired depth of cut and the second minimization was applied. Afterwards, the workpiece temperature was defined as 293 K, and the whole system was left for 25 ms and without any tool movement so that the final equilibration would be achieved. The MD calculations were performed under a micro-canonical (NVE) ensemble. Moreover, the equations of motion were integrated using the velocity–Verlet algorithm with the time steps of 1 fs. The simulations were carried out by a computer code, known as the large-scale atomic/molecular massively parallel simulator.[33] All the geometry and problem conditions were carried out by coding in this environment. Therefore, in addition to the extensive knowledge of molecular dynamics, it requires profound mastery of the simulation software as well as the basics of mathematics and physics. Also, to visualize and post-process the MD simulation data, the Open Visualization Tool[34] was employed. With the aid of this software, the surface characteristics, such as surface roughness and integrity, can be measured. The simulations were run on a high-performance computer with a total of 48 cores at the Yan laboratory, Keio University. The computing time for each simulation was between a few hours to 3 days. Details of the simulation parameters are given in Table I.

**Table I. Detailed parameters in the MD simulations**

**Workpiece parameters**

| | |
|---|---|
| Workpiece dimensions | 38.017 (length) × 19.0085(height) × 5.431(width) nm$^3$ |
| Length to height ratio | 2 |
| Initial temperature | 293 K |
| Number of workpiece atoms | 198,110 |
| Number of fixed atoms | 26,590 |
| Number of thermostatic atoms | 25,030 |
| Cutting plane and cutting direction | (001) [0$\bar{1}$0] |

| **Condition of nanometric cutting** | | **Tool parameters** | |
|---|---|---|---|
| Undeformed chip thickness | 0 nm–5 nm | Material | Rigid diamond |
| Cutting speed | 100 m/s | Tool edge radius | 1 nm, 3 nm, 5 nm |
| RTS | 0, 0.1, 0.25, 0.5, 0.75, 1 | Rake angle | − 10 |
| | | Clearance angle | 15 |
| Cutting distance | 20 nm | Number of atoms | 27,839 |

**Computational parameters**

| | | | |
|---|---|---|---|
| Interatomic interaction | Tersoff | Time step | 1 fs |

## RESULTS AND DISCUSSION

### Chip Formation

Figure 2 shows snapshots of MD simulations at different RTS ratios (according to supplementary table SI) for the tool with an edge radius of 3 nm. In all these conditions, there is no visible damage on the machined surface, which is in agreement with the previous experimental results with the same RTS range.[35] According to Fig. 2a, although the depth of cut is equal to 0 (RTS = 0), the machined surface is rubbed and affected. The reason for this lies in the adhesion of a layer of atoms on the tool surface. As shown in supplementary figure S1, due to Interatomic potential as well as the friction between the tool and workpiece particles, a number of surface atoms of the workpiece are attached to the tool and form a rigid region.[36] In fact, under this condition, this thin layer plays the role of a new tool edge with a very high rake angle and starts machining the workpiece.

However, the amount of this layer is not so large that it can form a chip; and it only degrades the surface roughness. It is important to underline that this thin layer is not a built-up edge, since, contrary to the definition of the built-up edge, this region only contains an atomic layer and does not grow over time. Moreover, there is no failure or separation of the atoms of this region with tool advancement.

Increasing the depth of cut to achieve a RTS of 0.1 changes the cutting mechanism from rubbing to ploughing (Fig. 2b). In this condition, apart from the adhered particles on the tool surface, a few of the atoms are pushed to front of the tool and make a very small adjunct. Supplementary figure S2 shows the surface production trend at this RTS and different cutting lengths. According to this figure, there is no change in the volume of this small chip with tool advancement; this is while the configuration of the atoms inside this volume is continuously changing. The reason for this lies in entering and exiting particles in this area during the process. As it is shown in supplementary figure S3, by tool advancement in the ploughing mechanism, a number of surface atoms tend to enter the chip area. On the other hand, due to the very low depth of cut here, the effects of the rubbing mechanism remain, and some atoms in front of the tool which previously moved in the chip area are pushed from this zone and slide below the tool. This phenomenon keeps the chip volume constant in the ploughing mechanism. The particles in this small chip affect the quality of the machined surface in two ways. First, by erratically separating some of the surface atoms, they reduce the surface quality, and, second, it acts like a quasi-BUE on the tool edge and causes surface deterioration. Therefore, in practice, nanometric cutting should be prevented from entering into this mechanism.

As shown in Fig. 2c, with a further increase in the RTS reaching 0.25, it is observed that the effective tool rake angle is closer to the nominal value and the extrusion mechanism becomes dominant. In this
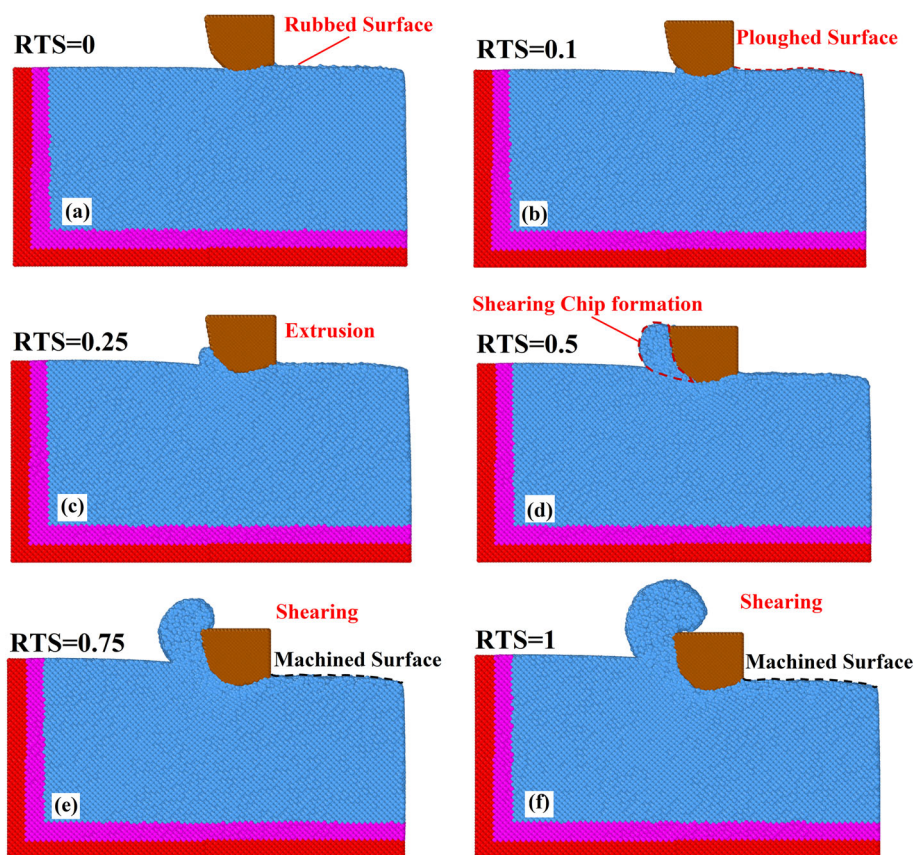
Fig. 2. The effect of RTS on chip formation mechanism (tool edge radius = 3 nm): (a) rubbing, (b) ploughing, (c) extrusion, and (d–f) shearing.

case, the surface quality is much better than the ploughing mode. In fact, the RTS = 0.25 can be defined as the minimum depth of cut for material removal in nanometric cutting.

By changing the RTS to 0.5, the cutting mechanism has been transformed from extrusion to shearing (Fig. 2d). Here, more portions of the surface atoms have been converted to chips. According to Fig. 2d–f, the remarkable point is that, by increasing RTS to 1, the same mechanism works and there is no marked change in the quality of the machined surface.

The chip formation mechanism for a 1-nm tool edge in different RTS ratios is shown in supplementary figure S4. By comparing these snapshots with those in Fig. 2, it is observed that, even under conditions of RTS = 0, the ploughing condition occurs. The reason is because particles are veering in front of the tool. As is illustrated in supplementary figure S5, the adhered layer on the tool surface decreases by reducing the tool edge radius. In this circumstance, this tiny layer plays the role of a new cutting edge, and, due to its sharpness, it breaks some atomistic bonds. Therefore, a number of atoms move to the front of the tool and form a very small chip. Nevertheless, a portion of these atoms can be rubbed beneath the tool and be a part of the machined surface. Thus, in this case, there will be no chip growth.

By early ploughing mechanism occurrence at RTS = 0, other cutting mechanisms also occur earlier than the 3-nm tool edge radius. The extrusion mechanism starts in a RTS of 0.1 in the tool edge of 1 nm (supplementary figure S4b). Moreover, by increasing the RTS to 0.25, a shearing mechanism starts to form. By increasing the RTS, the cutting mechanism completely enters into the shearing phase and the surface quality remains almost constant within the RTS = 0.5–1 range.

By comparing the cutting process in the tool with the edge radius of 5 nm to Fig. 2, it can be seen that no significant change has occurred in the production of different phases of cutting (supplementary figure S6). Nonetheless, the surface quality of the machined surfaces at the same RTS by the different tool edge radii is not the same. For instance, at RTS = 1 with the tool edge radius of 5 nm, the machined surface is profoundly affected, and even some edge swelling occurs (supplementary figure S6f). This is while, in the same conditions with the tool edge radius of 3 nm, surface integrity is much better and without any edge swelling (Fig. 2f). The reason is the lower hydrostatic pressure on the workpiece in the smaller tool radius.

As shown in Fig. 3, reducing the tool edge radius results in a lower depth of cut at the same RTS. This means that fewer atoms are stressed and, as a consequence, a smaller area in the workpiece is
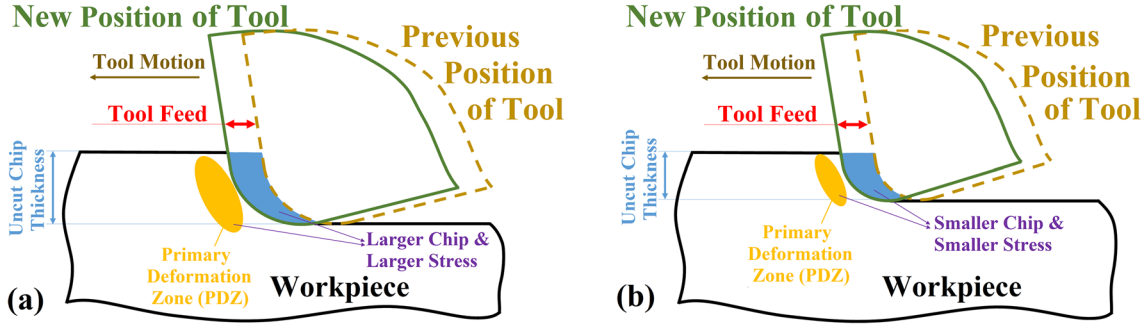
Fig. 3. The effect of tool edge radius on the machined surface at the same RTS and tool advancement, but at: (a) higher uncut chip thickness, and (b) lower uncut chip thickness.
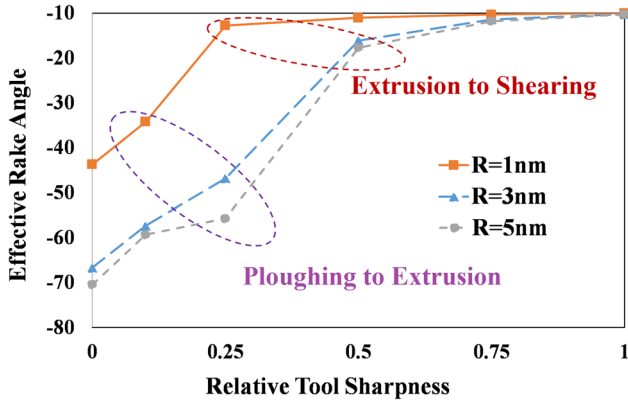


Fig. 4. Variation of the effective rake angle by RTS and tool edge radius.

affected. On the other hand, in the machining of brittle materials at a very low depth of cut, the plastic deformation flow is formed in front of the tool, called the primary deformation zone (PDZ).[37] By increasing the depth of the cut and, consequently, the relative tool sharpness, the size of the PDZ is also increased. In such conditions, a wider range of workpiece atoms are subjected to stress and, as a result, more deformation occurs on the atoms in front of and the bottom of the tool. In the meantime, the number of defects in front of the tool is increased by increasing the depth of cut; and this can be another factor in surface deterioration.[38]

In a blunt tool at minor RTS ratios, the effective tool rake angle would be different from the nominal rake angle in nanometric cutting. Hitherto, different theoretical definitions have been proposed by researchers. Lai et al.[20] stated that, when the depth of cut is lower than the tool edge radius (RTS is less than 1), the following equation can be used:

$$\gamma_{\text{eff}} = -\sin^{-1}\left(1 - \frac{d}{R}\right) \tag{3}$$

in which $d$ is the depth of cut and $R$ is the tool edge radius. However, these researchers themselves acknowledged that it is far from the real value.

Another theoretical equation was introduced by Wu et al.[10] in 2016 which was based on RTS:

$$\gamma_{\text{eff}} = \left[(1 - \text{RTS}) \times \sin^{-1}(1 - \text{RTS}) \right. \\ \left. + \sqrt{1 - (1 - \text{RTS})^2} - \frac{\pi}{2}\right] \bigg/ \text{RTS} \tag{4}$$

Some researchers believe that the actual effective rake angle is calculated from the stagnation point and tangent to the tool edge.[39] The same definition has been used in this research for the shearing and extrusion mechanism (supplementary figure S7a). Nonetheless, due to the different behavior of the particles in the two mechanisms of rubbing and ploughing, the mentioned definition could not be used anymore. By reducing RTS to these levels, there is no chip formation and, consequently, no stagnation point is formed in front of the tool. Therefore, in these two mechanisms, the effective rake angle is defined by the sliding angle (supplementary figure S7b).

Variation of effective rake angle in different RTS and tool edge radii are plotted in Fig. 4. It is monitored that, in all the three tool edges, the effective rake angle in the rubbing and ploughing mechanisms, in which there is no chip formation, are lower than −40°. Yan et al.[40] highlighted that, while the rake angle is more negative than −40°, the plane stress condition will be dominated and this promotes side flow of the materials instead of chip formation.

Moreover, increasing the depth of cut (or in the other words, the RTS), leads to closing the effective rake angle to the nominal rake angle. In such a situation, the stagnation point reaches the rake face (instead of the tool edge), and particles are following along it. The interesting point in this figure is that in all the three tool edges, during the transition from ploughing mechanism to extrusion, an incremental change has occurred in the trend. The reason for this is that, by starting extrusion, a large portion of the surface atoms, which previously were being rubbed through the tool bottom, has now entered the chip area. Extrusion to shearing transformation is started at RTS = 0.5 in the tool's edge radii of 3 nm and 5 nm. Again, another trend change can be seen in this step. Here, the intersection point of the tool rake face and the tool edge
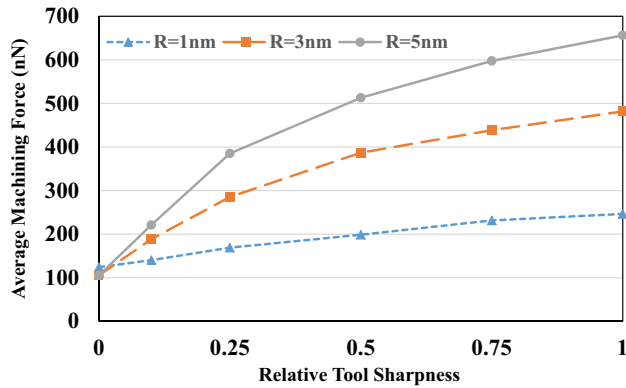
Molecular Dynamics Investigation of Nanometric Cutting of Single-Crystal Silicon Using a Blunt Tool


Fig. 5. The effect of RTS on average machining force.


Fig. 6. Machining forces and force angle during cutting.

reaches the depth of the cut. Accordingly, many more atoms flow to the chip. As shown earlier in supplementary figure S4, in a very sharp tool with a 1-nm edge radius, the mechanism of rubbing is not formed and, therefore, this mechanism transformation in this tool is different from the other two tools. In light of the fact that accessing the 1-nm tool edge is subject to limitations, we could introduce RTS = 0.25 as the ploughing to extrusion limit, and RTS = 0.5 as the extrusion to shearing. By starting chip formation in the shearing mechanism, it is observed that the increase of the RTS does not have much effect on the effective rake angle, and this amount ultimately leads to the nominal rake angle.

## Force Investigation

During the nanometric cutting, the cutting and thrust forces are constantly changing and severe fluctuation occurs. The main reason for this is the changes in atomic position in each step (due to chip formation and atomic vibration from the temperature).[31] Apart from that, the number and position of dislocations are changing at any moment, and this will affect the instantaneous machining forces. Thus, providing and investigating of these forces will not present very clear results. Consequently, the order 3 polynomial trendlines could be used for force fitting according to supplementary figure S8. This figure displays that an increase in the RTS will always result in growing the tangential and thrust forces due to the presence of more atoms in front of the tool, although the tangential force variation is excited by the growth rate and takes roughly the same trend, after about 12 nm. It happens because, after this tool advancement, the number of atoms between the machined surface and the clearance face reaches the maximum and, afterwards, remains constant (supplementary figures S9 and S10). Due to the fact that the rake and clearance angle are the same in all of these simulations, it can be concluded that the tool length for tangential force stability is independent of the RTS and depends solely on other tool parameters.
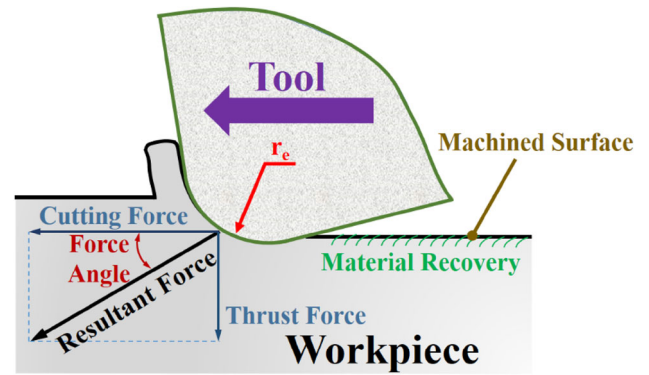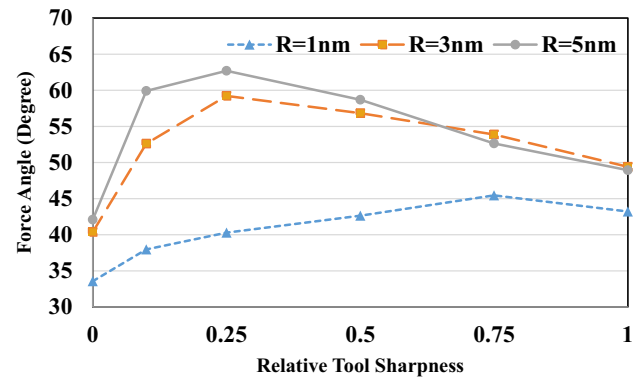

Fig. 7. The effect of RTS on force angle.

Approximately the same trend occurs for the thrust forces. Nevertheless, it can be seen that, unlike the tangential forces, this phenomenon has not occurred at the same cutting length. In fact, increasing the edge causes delays in the thrust force stability. This value is 9.3 nm, 14.6 nm, and 17.9 nm for tools with the edge radii of 1 nm, 3 nm and 5 nm, respectively.

Comparing the tangential and thrust forces during shearing mechanism in supplementary figure S8 demonstrates that the changes in the force trends in each tool are very similar to each other. This reveals that the particle behavior during the shearing mechanism is the same and the only difference is due to the number of atoms which should be pushed by the tool.

The effect of RTS and tool edge radius on average machining forces is displayed in Fig. 5, which illustrates that the machining forces at RTS = 0 and in two tools with the edge radii of 3 nm and 5 nm is almost the same. However, as the tool edge radius decreases to 1 nm, the machining mechanism has changed from rubbing to ploughing and this has led to an increase in the machining forces at this RTS.

By increasing the RTS and the transition of all the tools from the rubbing mechanism, it is seen that the sharper tool requires less machining force. It is also observed that the trend of the shearing

section in all three tools is very close to each other, and is about 189.7 nN.

Force angle is another important parameter in machining studies, which can affect the surface quality and machining forces. As shown in Fig. 6, force angle is defined as follows:

$$\theta_f = \tan^{-1} \frac{F_t}{F_c} \quad (5)$$

in which $F_c$ is tangential force (in direction of tool advancement) and $F_t$ is equal to the thrust force (perpendicular to the direction of tool advancement).

Figure 7 shows force angle variation in different RTS ratios and tool edge radii and illustrates that the lowest force angle has always occurred at RTS = 0. In this case, since there is no chip formation, the tangential force is much higher than the thrust force, and, as a consequence, the force angle is reduced to the lowest amount. In this circumstance, the frictional force on the one hand and the thermal deformation on the other cause plastic deformation at the surface of the workpiece and create a notable form error. By increasing RTS to 0.25 in the tools with edge radii of 3 nm and 5 nm, it is observed that the maximum force angle, equal to 59.21° and 62.69°, occurred in this case. This is due to the different nature of the chip formation in the extrusion mechanism. As mentioned earlier, although chips are produced in this mechanism, a large number of atoms in front of the tool are compressed (extruded) toward the tool bottom and form the new surface. This high pressure has increased the force angle to the maximum. By increasing the RTS in these two tools and entering into the shearing mechanism, the amount of these extruded atoms decreases and the force angle declines by 18.34°. At RTS = 0.75, the tool with the edge radius of 5 nm experiences a sharper reduction in force angle than the 3-nm tool edge. This happens because a portion of the chip moves to the top of the tool causing some surplus thrust force on the tool (supplementary figure S9). The changes in the trend of force angle for the tool with the edge radius of 1 nm is slightly different compared with the other two. The force angle increases with the RTS increasing to 0.75. In this situation, the force angle is 45.44° and the tangential and thrust forces are approximately equal. By increasing the depth of cut in this tool, a higher fraction of the cutting energy is applied to the tangential forces, which results in a lower force angle.

## CONCLUSION

MD simulation was used to explore the effect of RTS on chip formation mechanism in nanometric cutting of single-crystal silicon using a blunt tool. The main conclusions can be drawn as follows:

- Decreasing the RTS value could lead to different surface generation mechanisms, namely, shearing, extrusion, ploughing and rubbing.
- Despite the common belief, reducing the rake angle to the extremely negative values will not necessarily increase the ratio of the thrust force to the tangential force. It decreases dramatically by reducing the depth of the cut below a critical value.
- Even though there is no material removal at RTS = 0, the machined surface will be affected owing to material adhesion on the tool surface. In this situation, the dominant mechanism is rubbing and the utmost effective rake angle is produced.
- The cutting mechanism transforms to ploughing at RTS = 0.1. The minimum material removal occurs in the extrusion mechanism at the relative tool sharpness of 0.25. Extrusion to shearing mechanism occurs at RTS = 0.5.
- After a specific tool advancement, the tangential force reaches a maximum and there is almost no change in it. This distance is independent of the RTS. However, this concept does not work for thrust force and depends on the tool edge radius.

The findings from this study provide insights into the practical nanometric cutting processes and abrasive machining mechanisms of silicon wafers, and are useful to optimize the machining conditions for the best surface quality.

## ACKNOWLEDGEMENTS

## ELECTRONIC SUPPLEMENTARY MATERIAL

The online version of this article (https://doi.org/10.1007/s11837-019-03671-w) contains supplementary material, which is available to authorized users.

## REFERENCES

1. M. Heidari and J. Yan, *Int. J. Adv. Manuf. Technol.* 95, 479 (2018).
2. M. Mukaida and J. Yan, *Int. J. Mach. Tools Manuf* 115, 2 (2017).
3. V. Astakhop and J. C. Outeiro, in *Proceedings—8th CIRP International Workshop on Modeling of Machining Operations* (2005), p. 517.
4. X. Liu, R.E. DeVor, S.G. Kapoor, and K.F. Ehmann, *J. Manuf. Sci. Eng.* 126, 666 (2004).
5. F.Z. Fang and G.X. Zhang, *Int. J. Adv. Manuf. Technol.* 22, 703 (2003).
6. B.P. O'Connor, E.R. Marsh, and J.A. Couey, *Precis. Eng.* 29, 124 (2005).
7. M. Arif, Z. Xinquan, M. Rahman, and S. Kumar, *Int. J. Mach. Tools Manuf* 64, 114 (2013).

8. Z.J. Yuan, M. Zhou, and S. Dong, *J. Mater. Process. Technol.* 62, 327 (1996).
9. L. Zhanqiang, S. Zhenyu, and W. Yi, *Int. J. Adv. Manuf. Technol.* 69, 1219 (2013).
10. X. Wu, L. Li, M. Zhao, and N. He, *Int. J. Adv. Manuf. Technol.* 82, 1941 (2016).
11. M.A. Rahman, M.R. Amrun, M. Rahman, and A.S. Kumar, *Int. J. Mach. Tools Manuf* 115, 15 (2017).
12. M. Azizur Rahman, M. Rahman, and A. Senthil Kumar, *Int. J. Adv. Manuf. Technol.* 96, 3545 (2018).
13. J. Yan, T. Asami, H. Harada, and T. Kuriyagawa, *CIRP Ann. Manuf. Technol.* 61, 131 (2012).
14. J. Yan, H. Zhao, and T. Kuriyagawa, *Semicond. Sci. Technol.* 24, 75018 (2009).
15. D.C. Rapaport, *The Art of Molecular Dynamics Simulation*, 2nd ed. (Cambridge: Cambridge University Press, 2004).
16. R. Komanduri, N. Chandrasekaran, and L.M. Raff, *Philos. Mag. Part B* 79, 955 (1999).
17. M.B. Cai, X.P. Li, and M. Rahman, *Int. J. Mach. Tools Manuf* 47, 75 (2007).
18. A. O. Oluwajobi and X. Chen, in *Proceedings of Computing and Engineering Annual Researchers' Conference,* 1997 (2010), p. 160.
19. F.Z. Fang, H. Wu, W. Zhou, and X.T. Hu, *J. Mater. Process. Technol.* 184, 407 (2007).
20. M. Lai, X.D. Zhang, and F.Z. Fang, *Appl. Phys. A Mater. Sci. Process.* 108, 809 (2012).
21. S. Goel, N. Haque Faisal, X. Luo, J. Yan, and A. Agrawal, *J. Phys. D Appl. Phys.* 47, 275304 (2014).
22. V.A. Balogun, I.F. Edem, A.A. Adekunle, and P.T. Mativenga, *J. Clean. Prod.* 116, 187 (2016).
23. J. Ren, Z. Dong, J. Zhao, and P. Liu, *Appl. Surf. Sci.* 369, 584 (2016).
24. J. Guénolé, A. Prakash, and E. Bitzek, *Appl. Surf. Sci.* 416, 86 (2017).
25. S. Zare Chavoshi, S. Goel, and X. Luo, *J. Manuf. Process.* 23, 201 (2016).
26. H. Zhao, C. Shi, P. Zhang, L. Zhang, H. Huang, and J. Yan, *Appl. Surf. Sci.* 259, 66 (2012).
27. J. Li, Q. Fang, L. Zhang, and Y. Liu, *Appl. Surf. Sci.* 324, 464 (2015).
28. Y. Liu, B. Li, and L. Kong, *Comput. Mater. Sci.* 148, 76 (2018).
29. J. Tersoff, *Phys. Rev. B* 38, 9902 (1988).
30. J. Tersoff, *Phys. Rev. B* 37, 6991 (1988).
31. S.V. Hosseini and M. Vahdati, *Comput. Mater. Sci.* 65, 29 (2012).
32. H. Dai, G. Chen, C. Zhou, Q. Fang, and X. Fei, *Appl. Surf. Sci.* 393, 405 (2017).
33. S. Plimpton, *J. Comput. Phys.* 117, 1 (1995).
34. A. Stukowski, *Model. Simul. Mater. Sci. Eng.* 18, 085001 (2010).
35. J. Yan, T. Asami, H. Harada, and T. Kuriyagawa, *Precis. Eng.* 33, 378 (2009).
36. J. Shimizu, H. Eda, L. Zhou, and H. Okabe, *Tribol. Online* 3, 248 (2008).
37. G. Xiao, S. To, and G. Zhang, *Comput. Mater. Sci.* 98, 178 (2015).
38. S. Venkatachalam, O. Fergani, X. Li, J. Guo Yang, K.-N. Chiang, and S.Y. Liang, *J. Manuf. Sci. Eng.* 137, 021020 (2015).
39. G. Bissacco, H.N. Hansen, and J. Slunsky, *CIRP Ann. Manuf. Technol.* 57, 113 (2008).
40. J. Yan, M. Yoshino, T. Kuriagawa, T. Shirakashi, K. Syoji, and R. Komanduri, *Mater. Sci. Eng., A* 297, 230 (2001).